Negative Refraction at Infrared Wavelengths in a Two-Dimensional Photonic Crystal

A. Berrier,[1] M. Mulot,[1] M. Swillo,[1] M. Qiu,[1,*] L. Thylén,[1] A. Talneau,[2] and S. Anand[1,†]

[1]*Department of Microelectronics and Information Technology, Royal Institute of Technology, Electrum 229, S-16440 Kista, Sweden*
[2]*CNRS Laboratoire de Photonique et Nanostructures, Route de Nozay F-91460, Marcoussis, France*

(Received 12 January 2004; published 11 August 2004)

We report on the first experimental evidence of negative refraction at telecommunication wavelengths by a two-dimensional photonic crystal field. Samples were fabricated by chemically assisted ion beam etching in the InP-based low-index constrast system. Experiments of beam imaging and light collection show light focusing by the photonic crystal field. Finite-difference time-domain simulations confirm that the observed focusing is due to negative refraction in the photonic crystal area.

DOI: 10.1103/PhysRevLett.93.073902 PACS numbers: 42.70.Qs, 41.85.Ct, 42.25.Bs, 78.20.Ci

In the late 1960s, the properties of artificial materials with a negative value of the refractive index were imagined [1]: such materials would reverse Snell's law resulting in negative refraction of waves and they would not violate any physical principle. Some experiments proved the feasibility of such materials and showed negative refraction using microwaves [2–4]. However, it was far from obvious whether this unconventional phenomenon would scale down to the optical domain. In the meantime, the concept that photonic crystals could exhibit negative refraction in the optical regime without requiring a negative value of the permittivity ε and permeability μ started to gain ground [5]. Since their discovery in 1987 [6,7] photonic crystals (PhCs) have met a rapidly growing interest. Most of the PhC applications rely on the presence of a range of forbidden wavelengths in the crystal, known as the photonic band gap [8]. However, new physical phenomena in PhCs working outside the band gap were predicted [5,9,10]. In particular, negative refraction in PhCs was foreseen [5,11–14] and was just recently experimentally demonstrated at microwave wavelengths [15,16]. Simulations [14] showed that a planar two-dimensional (2D) PhC field can, as a result of negative refraction inside the crystal, act as a lens by focusing light both inside and beyond the field and very recently imaging by a 2D PhC field acting as a flat lens was shown in the microwave range [16]. However, no experimental evidence of all-angle negative refraction at infrared wavelengths has been provided yet, to the best of our knowledge.

In this Letter we demonstrate experimentally focusing of light due to negative refraction by a 2D PhC field at telecommunication wavelengths.

The 2D PhC studied here is a triangular lattice of air holes in a low-index contrast InP/GaInAsP/InP slab. The lattice constant is $a = 480$ nm and the hole radius is 125 nm. The band structures were calculated by the 2D finite-difference time-domain (FDTD) method for the transverse magnetic (TM) modes in the same way as in Ref. [17] in which the validity of the approximation of 3D FDTD band structures by 2D FDTD calculations with an effective index to account for the third dimension is described. The absorbing boundary conditions are perfectly matched layers. For the calculations, an effective index of 3.24 [17,18] was used for the background material. This value corresponds to the mode index of the fundamental guided mode of the InP/GaInAsP/InP slab around $\lambda = 1.55$ μm. The photonic band structure of the PhC for all in-plane wave vectors is shown in Fig. 1(a), while the photonic band structure for all the wave vectors along the edges of the irreducible Brillouin zone defined by the points Γ, M, and K is shown in Fig. 1(b).

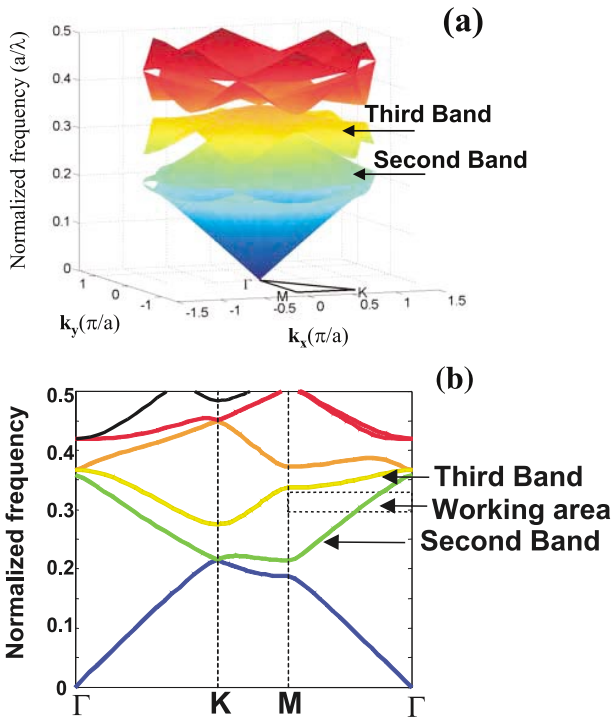

FIG. 1 (color online). Band structure and wave-vector diagram for the PhC structure: (a) calculated dispersion diagram showing the photonic band structure for all in-plane wave vectors and (b) photonic band structure at the edges of the irreducible Brillouin zone. The indicated working area shows the experimentally available wavelength range.

If we consider the photonic band structure of Fig. 1(a) at a given frequency, the resulting intersection defines the so-called equifrequency surface (EFS). It is well known that the propagation direction of light beams in any medium is given by the energy velocity vector $\mathbf{v_e}$. It has been proved that in PhCs, as for homogeneous media, the energy velocity vector is equal to the group velocity vector [19]. By definition the group velocity vector $\mathbf{v_g} = \nabla_k(\omega(\mathbf{k}))$ is always oriented perpendicular to the EFS in the direction along which $\omega(\mathbf{k})$ is increasing. Schematic wave-vector diagrams shown in Figs. 2(a) and 2(b) illustrate the direction of the wave propagation at an interface between two isotropic materials [Fig. 2(a)] and at an interface between an isotropic material and a photonic crystal [Fig. 2(b)].The wave vector $\mathbf{k}_1$ represents the incoming wave in material 1. The tangential components of $\mathbf{k}$ are always conserved at an interface between two materials. For any isotropic homogeneous material, the EFS is a circle with radius $|\mathbf{k}| = n\omega/c$, $\mathbf{k}$ being the wave vector, n the refractive index of the medium, ω the working frequency, and c the velocity of light *in vacuo*. However, for the photonic crystal, the shape of the EFS is frequency dependent. The working area in Fig. 1(b) represents the experimentally available wavelength range (1480–1610 nm), which corresponds to the reduced frequency (a/λ) range 0.298–0.325. The third band is out of this working wavelength range if the incident light is mainly along the ΓM direction. The EFS of the second band is almost circular in that frequency range. Therefore, the behavior of the PhC structure is isotropic-like. In the PhC case, when ω increases, the EFS moves inwards around the Γ symmetry point. Therefore, the group velocity vector points inwards resulting in negative refraction of the beam [Fig. 2(b)].

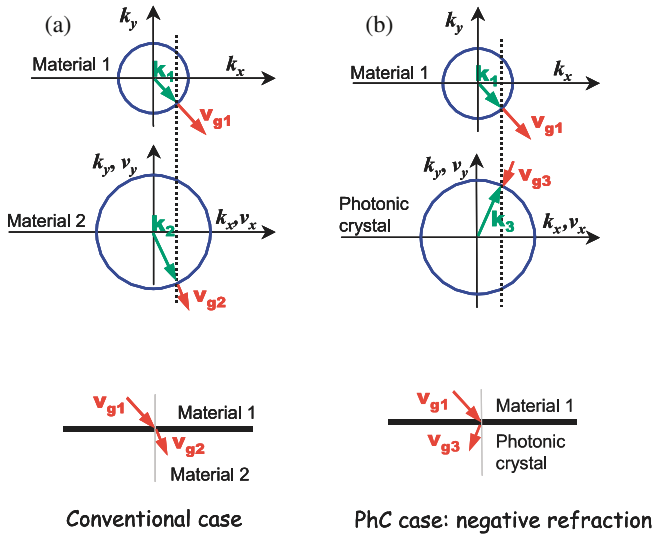

FIG. 2 (color online). Schematic wave-vector diagrams illustrate the propagation of the wave for the conventional case (a) and for the PhC case (b).

To demonstrate the negative refraction, we fabricated a device with the simulated eight-row air-hole triangular-lattice PhC field and a 1.2 μm wide input waveguide launching the input wave in the ΓM direction of the PhC. The PhC field is situated at a distance $d = 17$ μm from the cleaved facet (Fig. 3). The grown epitaxial structure is the low-index contrast planar waveguide InP/GaInAsP/InP. The thickness of the InP top layer and of the GaInAsP core layer are 200 and 420 nm, respectively. The PhC patterns were generated by electron-beam lithography, transferred into a SiO_2 mask and then etched into the semiconductor using Ar/Cl_2 chemically assisted ion beam etching [18]. The measurements on the structures are performed using the end-fire method: light is coupled into the waveguide through a polarization maintaining fiber, the output light is magnified with a microscope objective, while a polarizer ensures TM polarization. After passing through the PhC field the light travels in the material over the distance d and finally escapes from the sample through the cleaved facet. We image the light beam with the help of the microscope objective and a vidicon infrared camera. In that way we can record the beam intensity as a function of the lateral distance y and at different distances d from the cleaved facet, for $\lambda = 1480$ nm. Figures 4(a) and 4(b) show the recorded data from the beam imaging comparing the case without and with the PhC field, respectively. The increased value of the maximum intensity and the reduced full width at half maximum at 10 μm from the cleaved facet clearly demonstrate the focusing effect of the PhC field due to negative refraction, which is also confirmed by the FDTD simulation [20] (Fig. 5). A first focus area is located very close to the input interface, inside the PhC. The second focusing effect is taking place after the cleaved facet, in the air. The apparent splitting of the main output beam shaped by the PhC field is due to the following: (a) light is reflected at the III-V/air interface and interferes with the incoming light and (b) the output beam shaped by the PhC field is not a pure fundamental Gaussian beam. When increasing the wavelength, the focus area is moving towards the PhC field.

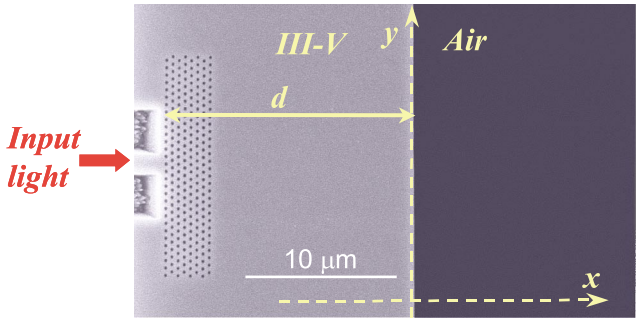

FIG. 3 (color online). Scanning electron microscope image of the fabricated device (top view).

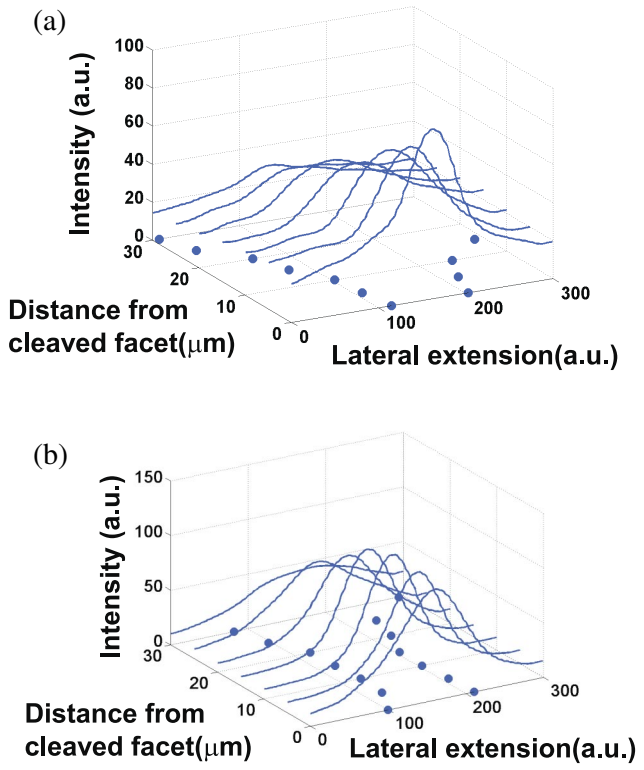

FIG. 4 (color online). (a) Measured light intensity distribution of the output beam, without the PhC field at different positions from the facet. (b) Measured light intensity distribution of the output beam with the PhC field. The evolution of full width at half maximum is plotted on the same graph with dots, showing the focusing of light ($\lambda = 1480$ nm).

As an extension of the above experiment, we fabricated a second device to demonstrate how negative refraction by the PhC could be used for light collection. The fabricated device is composed of (i) the eight-row air-hole triangular-lattice PhC field, (ii) the 1.2 μm-wide input ridge waveguide, and (iii) a 1.2 μm-wide collecting ridge waveguide placed at specific distances $d' = 14$ μm, $d' = 23$ μm, or $d' = 33$ μm from the input ridge end as shown in Fig. 6. For the purpose of comparison, we also fabricated a similar device but without the PhC field, with $d' = 24$ μm. Light is injected through the input waveguide in the same way as for the first set of experiments. The transmission spectra are normalized with respect to transmission through a reference ridge waveguide. The measured transmission curves are plotted in Fig. 7(a). For a given collecting position d' the intensity of the detected light reaches a maximum for a certain wavelength.

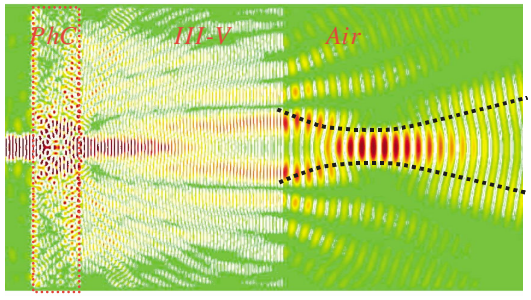

FIG. 5 (color online). Snapshot of the simulated light intensity distribution at $\lambda = 1480$ nm.

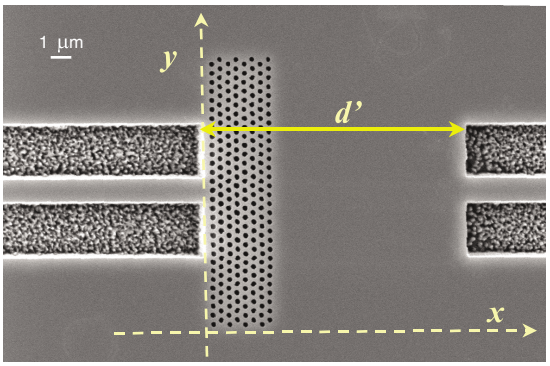

FIG. 6 (color online). Scanning electron microscope image of the device, with a collecting waveguide at $d' = 14$ μm (top view).

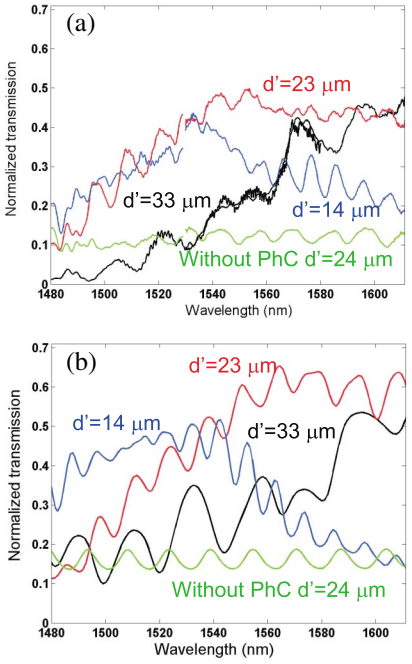

FIG. 7 (color online). (a) The experimental transmission spectra for different distances between input and collecting waveguides are $d' = 14$ μm, $d' = 23$ μm, and $d' = 33$ μm. The case without PhC is also plotted. Experimental data were obtained using two different broad-spectrum light sources, covering together the wavelength range 1480–1610 nm, performed in TM mode. (b) Simulated transmission spectra for the same values of d'.

Moreover, if we compare the cases with and without PhC field, we note that the intensity of light is significantly higher in the former case, which unambiguously shows that the PhC field is coupling the incoming light into the waveguide due to negative refraction. The maximum transmission for $d' = 33$ μm and $d' = 23$ μm is obtained from the simulation curves at wavelengths 1535 and 1595 nm, respectively. The focus point for $d' = 14$ μm is out of the available experimental range ($\lambda > 1610$ nm). This confirms that the focus position is shifted towards the PhC field as the wavelength increases. The oscillations on the transmission curves are due to a cavity effect between the edge of the PhC field and the edge of the collecting waveguide. The simulated transmission spectra were obtained by 2D FDTD using two line detectors which are placed in the input waveguide (reference) and in the output waveguide [21]. A pulse source is located at the entrance, before the input detector. We normalize the transmission spectra by comparing the Poynting vector at the reference and at the output detectors. The obtained curves are presented in Fig. 7(b). Comparing Figs. 7(a) and 7(b), we see that the measurement results are consistent with the simulations.

In conclusion, we have achieved light focusing at a telecommunication wavelength range using a PhC field fabricated in a low-index contrast system. This focusing is due to negative refraction of the incident light beam by the PhC field, which then acts like a flat lens. Two separate experiments were conducted: (a) imaging of the beam shaped by the photonic crystal and (b) transmission measurement through a collecting waveguide placed after the PhC field. The results from both the beam imaging experiment and the transmission experiment are consistent with predictions from the 2D FDTD calculations. Negative refraction is expected to be a significant step towards novel imaging optics and can lead to considerable changes in optical system design. It could also make possible 3D photography, open cavities, and novel coupling functionality in integrated optics components.

*Electronic address: min@imit.kth.se
†Electronic address: anand@imit.kth.se

[1] V. G. Veselago, Sov. Phys. Usp. **10**, 509 (1968).
[2] J. B. Pendry, Phys. Rev. Lett. **85**, 3966 (2000).
[3] R. A. Shelby, D. R. Smith, and S. Schultz, Science **292**, 77 (2001).
[4] D. R. Smith *et al.*, in *Photonic Crystals and Light Localization in the 21st Century*, NATO ASI, Ser. C, edited by C. M. Soukoulis (Kluwer Academic Publishers, Dordrecht, 2001), Vol. 563, pp. 351–371.
[5] M. Notomi, Phys. Rev. B **62**, 10 696 (2000).
[6] E. Yablonovitch, Phys. Rev. Lett. **58**, 2059 (1987).
[7] S. John, Phys. Rev. Lett. **58**, 2486 (1987).
[8] J. D. Joannopoulos, R. D. Meade, and J. N. Winn, *Photonic Crystals: Molding the Flow of Light* (Princeton University Press, Princeton, 1995).
[9] H. Kosaka *et al.*, Appl. Phys. Lett. **74**, 1212 (1999).
[10] S.-Y. Lin, V. M. Hietala, L. Wang, and E. D. Jones, Opt. Lett. **21**, 1771 (1996).
[11] B. Gralak, S. Enoch, and G. Tayeb, J. Opt. Soc. Am. A **17**, 1012 (2000).
[12] S. Foteinopoulou, E. N. Economou, and C. M. Soukoulis, Phys. Rev. Lett. **90**, 107402 (2003).
[13] M. Qiu, L. Thylén, M. Swillo, and B. Jaskorzynska, IEEE J. Sel. Top. Quantum Electron. **9**, 106 (2003).
[14] C. Luo, S. G. Johnson, J. D. Joannopoulos, and J. B. Pendry, Phys. Rev. B **65**, 201104 (2002).
[15] E. Cubukcu, K. Aydin, E. Ozbay, S. Foteinopoulou, and C. M. Soukoulis, Nature (London) **423**, 604 (2003).
[16] P. V. Parimi, W. T. Lu, P. Vodo, and S. Shridar, Nature (London) **426**, 404 (2003).
[17] M. Qiu, Appl. Phys. Lett. **81**, 1163 (2002).
[18] M. Mulot *et al.*, J. Vac. Sci. Technol. B **21**, 900 (2003).
[19] K. Sakoda, *Optical Properties of Photonic Crystals*, Springer Series in Optical Sciences Vol. 80 (Springer, New York, 2001).
[20] FDTD simulations are performed using the free software F2P: Finite-difference time-domain 2D simulator for Photonic devices, http://www.imit.kth.se/info/FOFU/PC/F2P/.
[21] M. Qiu, K. Azizi, A. Karlsson, M. Swillo, and B. Jaskorzynska, Phys. Rev. B **64**, 155113 (2001).